EFFECT OF SEISMIC BASE FAULT MOTION ON STRESS AND DEFORMATIONS IN SOIL DEPOSIT –A 3D NUMERICAL APPROACH –

by

Pradeep Kumar RAMANCHARLA* and Kimiro MEGURO†

ABSTRACT

This paper contributes to understand the response of soil deposits due to underlying bedrock fault displacement in three dimensions. When an active bedrock fault ruptures, the movement along the fault propagates through the overlying soil and produces zones of intense shear. Hence, it is important to study the surface behaviour based on the fault characteristics. For this reason, we attempted to develop a new application to Applied Element Method (AEM) by modelling the fault rupture zone. In this paper, we model the fault rupture problem in three dimensions. First, a simple model is used to illustrate the absorption of the bedrock deformation by the overlying soil in elastic case. The results are compared with the analytical and numerical models wherever applicable. In the later part, the non-linear analysis is carried out to study the complex failure propagation in three dimensions. Influence of mechanical properties of the material is also discussed.

INTRODUCTION

Although there has been some improvement in our understanding over the last few decades, a complete understanding of the phenomenon of fault rupture propagation in three dimensions may never be achieved due to the complexities of the geological processes and materials involved. For example, there is a need to relate the rupture and the ground surface deformation. The common practice with important facilities such as dams, nuclear power plants and public buildings has been to avoid construction across the recognized trace of an active fault. However, in case of the buried faults our ability to delineate the possible potential hazard that can be caused due to the future rupture activity is far from complete. Additionally, it is important to quantify the displacement field in the vicinity of the fault trace.

Two enormously disastrous earthquakes occurred during the year 1999. The first one was an earthquake of magnitude 7.4 (Mw) occurred in Turkey on 17th August 1999[1)], and immediately following that, another event of magnitude 7.3 (Mw, Central Weather Bureau, Taiwan) occurred in Taiwan on 21st September 1999[2)]. The earthquake fault (North Anatolian Fault) in Turkey was traced over 100 km. The magnitude of right lateral movement of the fault on the ground surface was measured to be 2 to 4 m. And in Taiwan, severer effects were observed. The earthquake fault (Cher-Lung-Pu Fault) was traced for about 80 km, here the fault movement directly caused severe damage. The magnitude of maximum vertical differential movement was measured to be nearly 10.0 m. From the above two events, it is clear that the severe damage can be caused not only by the strong ground motion but also due to large surface deformations lying directly over the seismic

* Post Doctoral Fellow, Institute of Industrial Science, The University of Tokyo
† Assoc. Professor, International Center for Urban Safety Engineering, Institute of Industrial Science, The University of Tokyo

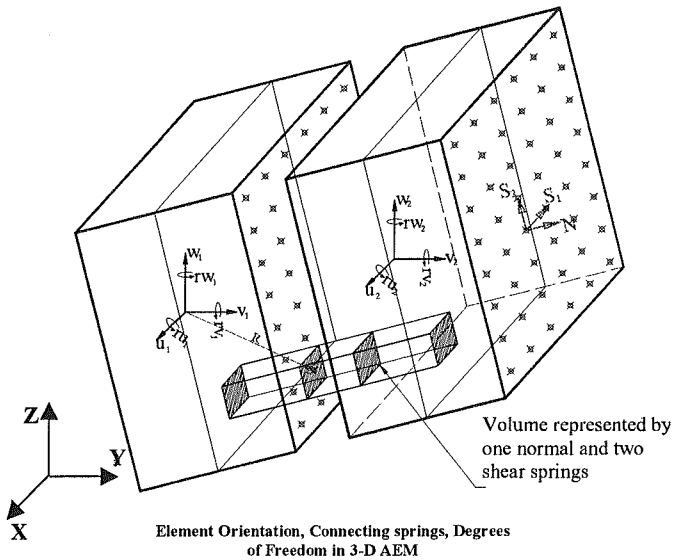

Element Orientation, Connecting springs, Degrees of Freedom in 3-D AEM

Fig. 1 Element formulation in 3D-AEM

Table 1 One quarter of stiffness matrix

	(1)	(2)	(3)	(4)	(5)	(6)
(1)	$K_nN_x^2$ $+K_{1s}S_{1x}^2$ $+K_{2s}S_{2x}^2$	$N_xK_nN_y$ $+S_{1x}K_{1s}S_{1y}$ $+S_{2x}K_{2s}S_{2y}$	$N_xK_nN_z$ $+S_{1x}K_{1s}S_{1z}$ $+S_{2x}K_{2s}S_{2z}$	$K_nN_x(R_yN_z-R_zN_y)$ $+K_{1s}S_{1x}(R_yS_{1z}-R_zS_{1y})$ $+K_{2s}S_{2x}(R_yS_{2z}-R_zS_{2y})$	$K_nN_x(R_zN_x-R_xN_z)$ $+K_{1s}S_{1x}(R_zS_{1x}-R_xS_{1z})$ $+K_{2s}S_{2x}(R_zS_{2x}-R_xS_{2z})$	$K_nN_x(R_xN_y-R_yN_x)$ $+K_{1s}S_{1x}(R_xS_{1y}-R_yS_{1x})$ $+K_{2s}S_{2x}(R_xS_{2y}-R_yS_{2x})$
(2)	S(1,2)	$K_nN_y^2$ $+K_{1s}S_{1y}^2$ $+K_{2s}S_{2y}^2$	$N_yK_nN_z$ $+S_{1y}K_{1s}S_{1z}$ $+S_{2y}K_{2s}S_{2z}$	$K_nN_y(R_yN_z-R_zN_y)$ $+K_{1s}S_{1y}(R_yS_{1z}-R_zS_{1y})$ $+K_{2s}S_{2y}(R_yS_{2z}-R_zS_{2y})$	$K_nN_y(R_zN_x-R_xN_z)$ $+K_{1s}S_{1y}(R_zS_{1x}-R_xS_{1z})$ $+K_{2s}S_{2y}(R_zS_{2x}-R_xS_{2z})$	$K_nN_y(R_xN_y-R_yN_x)$ $+K_{1s}S_{1y}(R_xS_{1y}-R_yS_{1x})$ $+K_{2s}S_{2y}(R_xS_{2y}-R_yS_{2x})$
(3)	S(1,3)	S(2,3)	$K_nN_z^2$ $+K_{1s}S_{1z}^2$ $+K_{2s}S_{2z}^2$	$K_nN_z(R_yN_z-R_zN_y)$ $+K_{1s}S_{1z}(R_yS_{1z}-R_zS_{1y})$ $+K_{2s}S_{2z}(R_yS_{2z}-R_zS_{2y})$	$K_nN_z(R_zN_x-R_xN_z)$ $+K_{1s}S_{1z}(R_zS_{1x}-R_xS_{1z})$ $+K_{2s}S_{2z}(R_zS_{2x}-R_xS_{2z})$	$K_nN_z(R_xN_y-R_yN_x)$ $+K_{1s}S_{1z}(R_xS_{1y}-R_yS_{1x})$ $+K_{2s}S_{2z}(R_xS_{2y}-R_yS_{2x})$
(4)	S(1,4)	S(2,4)	S(3,4)	$K_n(R_yN_z-R_zN_y)^2$ $+K_{1s}(R_yS_{1z}-R_zS_{1y})^2$ $+K_{2s}(R_yS_{2z}-R_zS_{2y})^2$	$K_nN_x(R_yN_z-R_zN_y)$ $(R_zN_x-R_xN_z)$ $+K_{1s}S_{1x}(R_yS_{1z}-R_zS_{1y})$ $(R_zS_{1x}-R_xS_{1z})$ $+K_{2s}S_{2x}(R_yS_{2z}-R_zS_{2y})$ $(R_zS_{2x}-R_xS_{2z})$	$K_n(R_yN_z-R_zN_y)$ $(R_xN_y-R_yN_x)$ $+K_{1s}(R_yS_{1z}-R_zS_{1y})$ $(R_xS_{1y}-R_yS_{1x})$ $+K_{2s}(R_yS_{2z}-R_zS_{2y})$ $(R_xS_{2y}-R_yS_{2x})$
(5)	S(1,5)	S(2,5)	S(3,5)	S(4,5)	$K_n(R_zN_x-R_xN_z)^2$ $+K_{1s}(R_zS_{1x}-R_xS_{1z})^2$ $+K_{2s}(R_zS_{2x}-R_xS_{2z})^2$	$K_n(R_xN_y-R_yN_x)$ $(R_xN_y-R_yN_x)$ $+K_{1s}(R_zS_{1x}-R_xS_{1z})$ $(R_xS_{1y}-R_yS_{1x})$ $+K_{2s}(R_zS_{2x}-R_xS_{2z})$ $(R_xS_{2y}-R_yS_{2x})$
(6)	S(1,6)	S(2,6)	S(3,6)	S(4,6)	S(5,6)	$K_n(R_xN_y-R_yN_x)^2$ $+K_{1s}(R_xS_{1y}-R_yS_{1x})^2$ $+K_{2s}(R_xS_{2y}-R_yS_{2x})^2$

faults. Hence, it is necessary to direct our efforts to study the relation between seismic fault characteristics, thickness of soil deposit and surface deformation.

Many researchers conducted experiments to understand the phenomena of surface failure, Cole and Lade[3] have tried to determine the location of surface fault rupture and width of the affected zone in alluvium over dip-slip fault using fault test box. They hypothesized that the results may be applicable to cohesive materials. Lade et al.[4] studied to determine the multiple failure surfaces by conducting the experiments on sand using fault test box. The results of the sand box model tests concluded that the observed displacement fields were largely the same for the different materials. Onizuka et al.[5] have modelled the deformation of ground using aluminium rods. Through experiments, they investigated bedrock stresses induced by reverse dip-slip faults. Bray and co-workers[6] investigated the pattern of ruptures in clay models under 1 g subjected to dip-slip faulting. The range of bedrock's dip angle varied from 60^0 to 90^0 for both normal and reverse faults. Tani et al.[6] conducted a 1-g model study of dip-slip faulting using dry Toyoura sand as model material.

Results from their first series of tests indicated that the base offset necessary for the rupture to propagate to the ground surface varied with fault orientation. These observations are in agreement with those from the study of Cole and Lade[3].

Using the above experimental methods, we can find the influence length. However, replicating the actual field conditions using experiments is very difficult, especially, controlling the material properties and modelling the boundary conditions. Moreover, large amount of data is necessary to establish a relationship between seismic fault parameters and resulting surface deformation. On the other hand, studying this phenomenon using numerical model has the advantage of controlling the parameters like material properties, size of the model, boundary condition, dip angle, etc. Numerical model allow us to investigate a number of aspects of the fault rupture propagation phenomenon, which are difficult to study from the examination of case histories or the conduct of physical model tests.

The discrete element approach intuitively looks promising. A soil mass is not a continuum. Instead, it is an assemblage of finite-sized particles. Inter-particle forces fundamentally determine the observed macroscopic behaviour of soil. Moreover, once a shear or tension cracks develop within the soil mass, it typically becomes difficult to reliably apply a numerical approach based on the principles of continuum mechanics. The EDEM (Extended Distinct Element Method), however has a serious drawback in that it requires an enormous amount of calculation time because explicit numerical integration is unstable unless the time increment used is very short[8].

APPLIED ELEMENT METHOD (AEM)

Here the extension of AEM[6),7)] to three dimensions is explained briefly. Two elements shown in **Fig. 1** are assumed to be connected by the sets of one normal and two shear springs. Each set is representing the volume of elements connected. These springs totally represents stress and deformation of that volume of the studied elements. Six degrees of freedom are assumed for each element. These degrees of freedom represent the rigid body motion of the element. Although the element motion is as a rigid body, its internal deformations are represented by spring deformation around each element. This means that the element shape doesn't change during analysis, but the behaviour of element collections is deformable.

To have a general stiffness matrix, the element and contact spring's locations are assumed in a general position. The stiffness matrix components corresponding to each degree of freedom are determined by assuming a unit displacement in the studied degree of freedom direction and by determining forces at the centroid of each element. The element stiffness matrix size is only (12 x 12). **Table 1** shows the components of the upper left quarter of the stiffness matrix. It is clear that the stiffness matrix depends on the contact spring stiffness and the spring location. The stiffness matrix given in **Table 1** is for only one pair of contact springs. The global stiffness matrix is determined by summing up the stiffness matrices of individual pair of springs around each element. Consequently, the developed stiffness matrix is an average stiffness matrix for the element according to the stress situation around the element. By using the advantage of AEM's simplicity in formulation and accuracy in non-linear range[7)], fault rupture zone shown in **Fig. 2** is modelled.

MODEL PREPARATION

There are three main types of faults, categorized according to the relative movement between the displaced bedrocks blocks: Strike-slip, dip-slip and thrust faults. In order to discuss the effect of strike slip faults on the surface, we need to carry out the investigation using 3D model. Hence, our attention is to show a new application of numerical model 3D-AEM. **Figure 2** shows the numerical

model representing the left lateral strike slip fault. This model is used to study the fault rupture propagation for strike slip faults. The model is prepared by using 2400 cube-shaped elements. Total size of the model is 120x250x80 m and number of elements in each of the directions is 12x25x8. The number of connecting springs in each face of the element are 25. Since this is the preliminary study, small size of the model is used.

Generally, soil strata and bedrock extend upto tens of kilometres in horizontal direction. Numerical modelling of such a large media is a difficult task and moreover, for studying the surface behaviour near the active fault region, it is necessary to model the small portion of the region that will include all the effects when the bedrock moves. For studying the selected region numerically, we assumed the boundary on left side to be fixed. Bottom of the model is treated as bedrock and left half of which is treated as fixed boundary and the right half is movable.

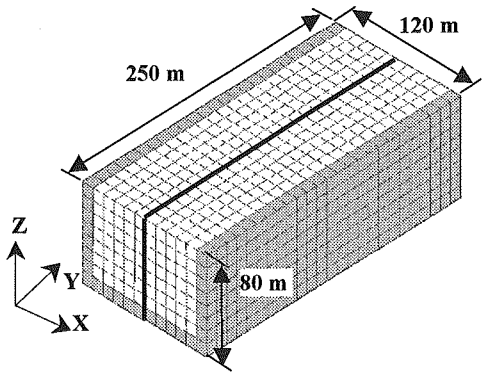

Fig. 2 Numerical model for studying strike slip faults

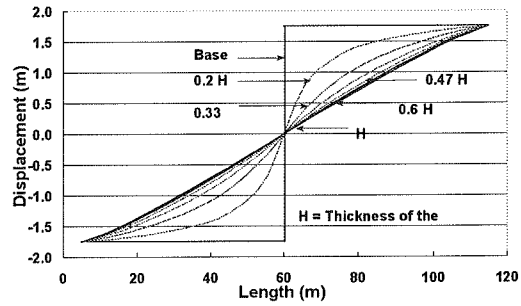

Fig. 3 Centre line deformation at various depths in the deposit

LINEAR MODELLING OF FAULTS

Analysis is carried out by giving the displacement equal to 5% (i.e. 3.5 m) of the thickness of the deposit. Young's modulus of the deposit is taken as 2.5×10^5 kN/m^2. **Figure 3** shows the deformation of the centre line at various depths in the deposit. From this figure, it can be seen that the deformation is absorbed inside the deposit. Originally the elements in a straight line attain different deformations at different heights. At the bottom of the deposit near the bedrock, the total offset is seen. However, when we move towards the ground surface, deformation becomes less. The reason for this is the elastic properties. The mechanical properties of the surficial materials sheared by the fault can significantly affect the surface deformation pattern. The inherent deformability of soils ensures that a fraction of the total offset across a distinct base rock fault (occurring commonly in a narrow zone) will be distributed across a relatively larger mass of overlying deformed soil, and hence, the distinct offset at the ground surface will be typically less than that at the bedrock-soil contact. This effect depends on the properties of the material overlying the active fault. These observations may prove important in developing effective techniques to mitigate faulting induced damage. For example, on the one hand,

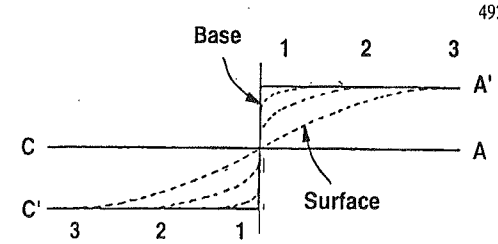

Fig. 4 Interpretation of the distribution in plan view of a distinct base offset propagating in overlying deformable deposit (Reid, 1910)

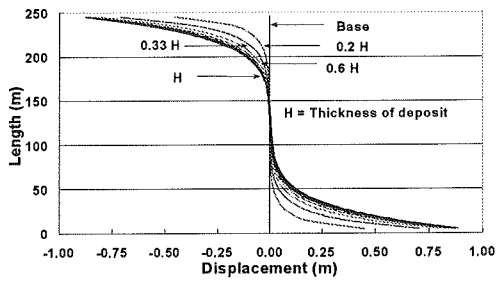

Fig. 5 Deformation at various depths in the deposit

a ductile compacted fill placed over a potentially active bedrock fault will partly absorb the distinct base fault movement as deformation. Therefore, the surface differential movements and extensional strains in this zone will be smaller. However, the base fault offset will be distributed across a relatively wide area, possibly affecting numerous neighbouring structures. On the other hand, a stiffer, more brittle fill overlying the fault one will tend to concentrate that distinct base rock offset in a narrower area, and transfer more of the base offset to the ground surface.

Based on analyses of the resulting patterns of surface deformation after the 1906 San Francisco earthquake, Reid[5] rendered an early and clear interpretation of the simultaneous occurrence of fractures and deformation in a deformable soil being sheared by an underlying bedrock strike-slip fault movement (see **Fig. 4**). Originally straight, horizontal lines at various depths in the deposit along line "C-A" attains different positions i.e., "C'-A', 1-1, 2-2, and 3-3", after the bedrock fault ruptures. The key observation Reid made was that the overlying soil could absorb part of the distinct base offset as deformation, thus generating a complex interaction of individual fractures and global shear deformation. Apparently, for more deformable, or equivalently, more ductile soils, larger base offsets can be absorbed before the ground surface ruptures.

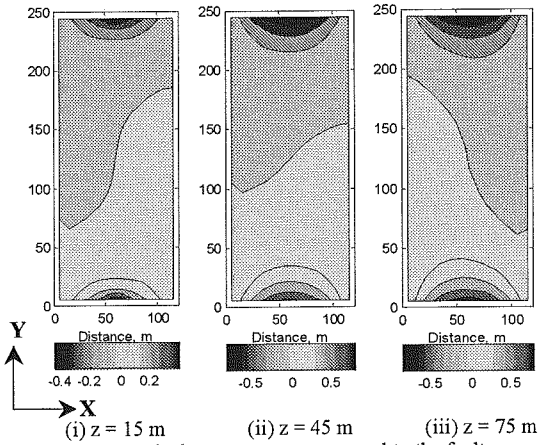

(i) z = 15 m (ii) z = 45 m (iii) z = 75 m

(a) Displacement contour normal to the fault

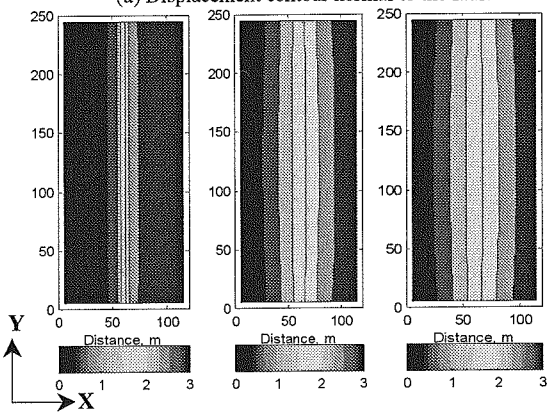

(i) z = 15 m (ii) z = 45 m (iii) z = 75 m

(b) Displacement contour parallel to the fault

Fig. 6 Deformation contours at various depths in the deposit

STRESSES AND STRAIN CONTOURS AT DIFFERENT SECTIONS

Figure 5 shows the horizontal deformation of the straight line just adjacent to the place where the rupture is taking place. From this figure, it can be seen that the line initially straight near the bedrock, deforms in the horizontal direction perpendicular to the plane of rupture. This deformation increases as we move from the bedrock towards the ground surface. When we closely look at this phenomenon in three dimensions, we can see that it is producing Reidel shear pattern. In order to have the detailed understanding of this phenomenon, let us look at the displacement field inside the deposit. **Figure 6** shows the displacements at various levels (15m, 45m and 75m) normal to the fault (see **Fig. 6 (a)**) and parallel to the fault (see **Fig. 6 (b)**) directions, respectively. From the displacement normal to the fault shown in **Fig. 6 (a),** it can be seen that at the height 15 m from bedrock, the displacement is positive at one end and negative at the other end. This is due to the anti-clockwise moment produced by the movement of left lateral strike-slip fault. This lateral displacement normal to the fault increases when we move towards the surface, as shown in **Fig. 6 (a)** at 45 m and at 75 m. On observing the displacement parallel to the fault shown in **Fig. 6 (b)**, we can easily see that the deformation is uniform over the length of the fault in the close proximity of

the bedrock. However, when we move towards the surface, this deformation reduces slightly at both the ends. The reason for this is the magnitude of shear stresses that reduces near the surface at both the edges. When we look at the **Fig. 6 (b)**, it can easily be observed that the displacement parallel to the fault increases towards the boundary. The magnitude of this displacement is maximum near the bedrock and reduces towards the surface.

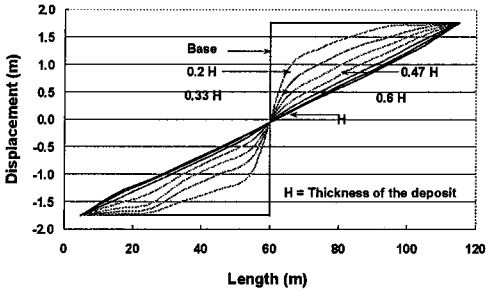

Fig. 7 Base line deformation at various depths using AEM

NON-LINEAR MODELLING OF FAULTS

Material properties adopted for non-linear analysis are: Young's modulus, $E = 2.5 \times 10^5$ kN/m^2, tensile strength, $\sigma_t = 1.5 \times 10^3$ kN/m^2 and compressive strength, $\sigma_c = 1.5 \times 10^4$ kN/m^2.

(a) Pure strike slip fault

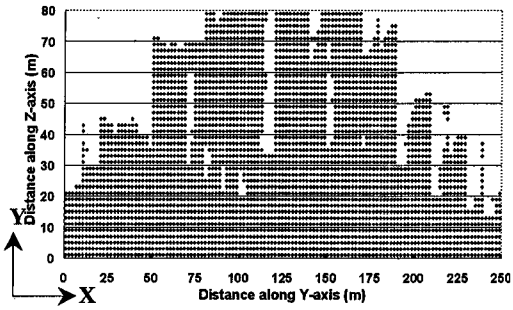

Fig. 8 Propagation of cracks along center line

The amount of base offset necessary for a strike slip fault to propagate to the ground surface can be a critical factor when siting astride an active fault. This parameter, which depends on the mechanical properties of the surficial materials, also depends on the kinematic and geometric constraint of the problem. However, although kinematic and geometric effects play a major role in fault rupture propagation through soil, they have not been adequately studied and quantified[11]. As with various problems in geotechnical engineering, rupture patterns can be significantly influenced by kinematic boundary conditions. Geometric effects can be also important. For instance, the amount of bedrock offset necessary for the rupture to be expressed at the ground surface depends on the thickness and geometry of the soil deposit or earth structure being ruptured by the underlying fault. To advance our understanding of surface faulting, it is necessary to identify the controlling factors in the fault process. Among all the factors, that affect the phenomenon characterizing surface rupture, the most important factors are: (1) the type of fault movement (normal, reverse, strike-slip), (2) the inclination of the fault plane, (3) the amount of displacement along the fault, (4) the depth and geometry of the overlying earth materials, (5) the characteristics of the overlying earth materials, and (6) the history of faulting, which includes fault age, slip-rate, and the maximum offset per event.

An interesting observation provided by Naylor et al.[13] was three-dimensional reconstruction of individual shear ruptures. They noticed that because of the existing kinematic conditions (i.e., a concentrated fault at the base and the overall shear movement), adjacent en echelon R shears evolved from disconnected segments at the surface to a single rupture at the base. Therefore, it can be hypothesized that at the surface the orientation of the initial R shears was influenced by dilatancy and possibly strength of the sand; whereas near the base this orientation was solely governed by the existing kinematic boundary conditions.

Figure 7 shows the base line deformation at various depths in the soil deposit. This figure is similar to **Fig. 3** except for the case of non-linearity of the material property. In this figure, it can be seen that the absorption of deformation inside the deposit is not like in elastic case. Here the cracks generated when the stresses inside the material reached the material capacity. **Figure 8** shows the propagation of cracks along the centre line. Each point in this figure is indicating the location of

failure spring, which in turn indicates the location where the maximum shear is taking place. It can be understood from this figure, that the maximum shear is taking place near the base rock and as we move to the surface its influence is getting concentrated in the narrow zone. This effect can be clearly understood when we look at the crack pattern observed on the ground surface. **Figure 9** shows the evolution of the cracks from the bedrock upto the surface. From this set of 4 figures, it can be clearly seen that the cracks that are distributed in the wider zone near the bedrock become concentrated in the smaller zone when they reach the surface. This figure clearly indicates the evolution of en echelon pattern. And more clear view of the crack distribution on the ground surface can be seen in **Figure 10**.

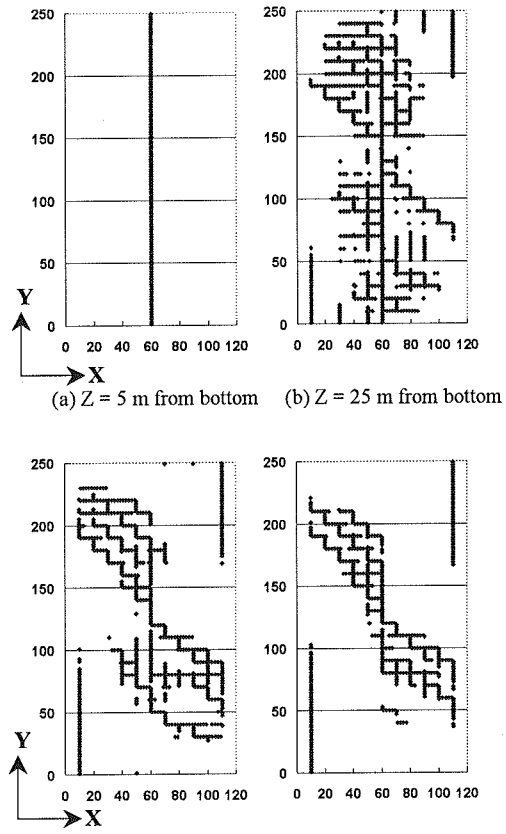

(a) Z = 5 m from bottom (b) Z = 25 m from bottom

(c) Z = 55 m from bottom (d) Z = 75 m from bottom

Fig. 9 Evolution of cracks from bedrock to the ground surface

(b) Effect of stiffness of soil deposit

As such, deformable capacity of soil depends on both stiffness and strength. However, studying the combined effect will be complicated. Hence for simplicity, we considered the effect of each while considering the other parameter as constant.

To check the effect of elastic material properties on the deformation of the deposit, two cases are studied by changing the stiffness of the deposit. Displacement of 5% of the thickness of the deposit is given to the movable block. First, the modulus of elasticity is increased, i.e. the analysis is carried out using relatively harder material i.e., $E=5x10^5$ kN/m^2. **Figure 11 (a)** shows the centre line deformation and **Fig. 11(b)** shows the crack patterns observed on the surface. From **Fig. 11 (a),** it can be seen that the deformation of the centre line at various depths is not same as the deformation pattern for elastic case as shown in **Fig. 3**. This is due to the brittleness of the material. From this, it is clear that harder material tends to transfer more base offset to the ground. This can be more clearly understood if we observe **Fig. 11 (b)**. In this, the crack that is parallel to the fault near the bedrock rotates and intersects the centre line at nearly 45 degrees. In this case, the cracks are concentrated and intersect the base line. Where as in the earlier case as shown in **Fig. 9** two cracks form the en echelon pattern. This means that if the material is softer, more deformation is absorbed inside the soil deposit and there can be clear appearance of the en echelon pattern. To discuss this effect, analysis is carried out by reducing the material stiffness i.e. $E=1.25x10^5$ kN/m^2. **Figures 12 (a)** and **(b)** are similar to **Figs. 11 (a)** and **(b)**. From these set of figures, it can be easily understood that due to the deformable capacity, more base offset is absorbed inside the deposit, thus affecting the wide

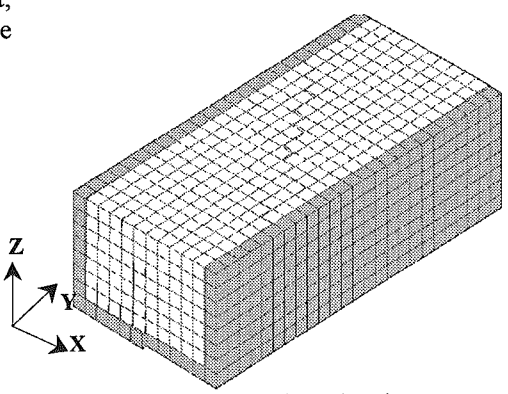

Fig. 10 Element location and cracks patterns

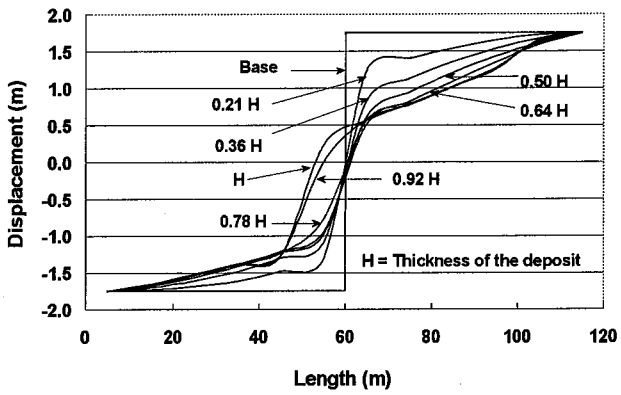

(a) Base line deformation at various depths

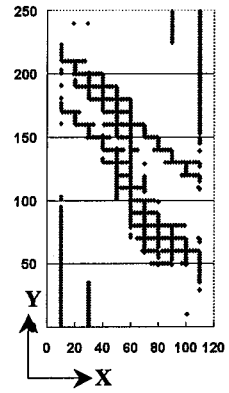

(b) Cracks on the ground surface

Fig. 11 Effect of elastic material property (**Case 1**)

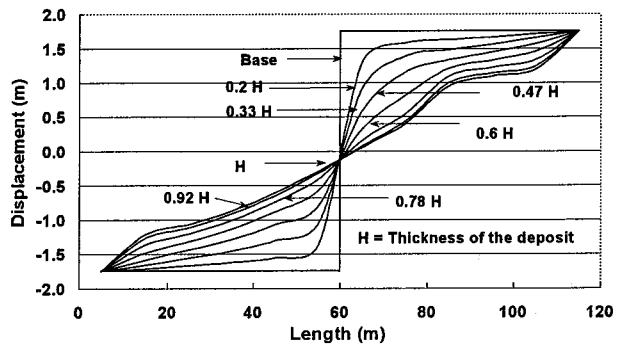

(a) Base line deformation at various depths

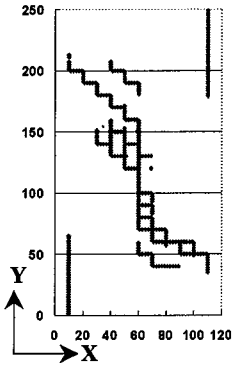

(b) Cracks on the ground surface

Fig. 12 Effect of elastic material property (**Case 2**)

area on the surface. From the figure, clear appearance of en echelon pattern on the surface can be seen.

(c) Effect of strength of the soil deposit

Strength is another important parameter on which the evolution of the surface rupture from the seismic bedrock depends. To understand this, analysis is carried out by reducing the material strength to 50% and keeping the stiffness same as in case of **Figs. 9** and **10**. Displacement of 5% of the thickness is given to the movable block and the effects are observed. **Figure 13** shows the final crack pattern on the surface after the total deformation of the base fault. From this figure, it can be observed that, due to the reduced strength, the number of failed springs are more compared to the previous case as explained in **Fig. 9**.

(d) Effect of thickness of the soil deposit

Thickness of overlying soil deposits can be different in different places where the faults are buried. For the similar movement of the buried fault, these deposits can produce different effects on the surface deformation. Hence, analysis is carried out to find the influence of the thickness of the deposit on the distribution of the cracks on the surface. Model size of 120x250x60 m is considered for the analysis. Material properties are same as in case of **Figs. 9** and **10**. Pure strike of 1.75 m is

given to each block. **Figure 14** shows the crack distribution on the ground surface. From this figure, it can be easily said that for the same amount of slip, the faults that are buried at shallower depths can produce more cracks on the ground surface than that faults seated and greater depths.

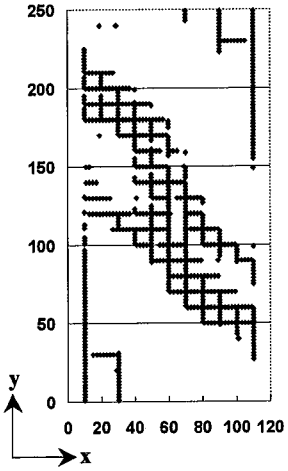

Fig. 13 Effect of strength

CONCLUSIONS

A new application to the 3D AEM is developed in this paper. By using a preliminary model, fault rupture propagation is studied in elastic and non-linear cases. From the results, it can be concluded that the deformable soil deposit will partly absorb the distinct base offset. However, the base fault offset will be distributed across relatively wider area, possibly affecting numerous neighbouring structures. On the stiffer soil deposits, more cracks are exposed on the surface where as in the softer soil more deformation is absorbed inside the deposit resulting less cracks on the surface. In case of thinner overlying deposits, more number of cracks exposed on the surface for same bedrock displacement compared to thicker deposits.

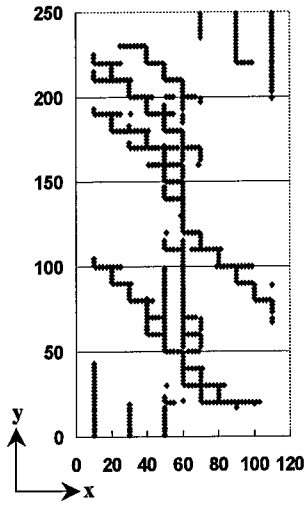

Fig. 14 Effect of thickness

REFERENCES

1) Japan Society of Civil Engineers, *The 1999 Kocaeli earthquake, Turkey, Investigation into damage to civil engineering structures*, Earthquake Engineering Committee, Japan Society of Civil Engineers, 1999 (a).
2) Japan Society of Civil Engineers, *The 1999 Ji-Ji earthquake, Taiwan, Investigation into damage to civil engineering structures*, Earthquake Engineering Committee, Japan Society of Civil Engineers, 1999 (b).
3) Cole, D. A., Jr., and Lade, P. V., Influence zones in alluvium over dip-slip faults, Journal of Geotechnical Engineering, ASCE, Proc. Paper 18788, Vol. 110, No. GT5, pp. 599-615, 1984.
4) Lade, P. V., Cole, D. A., Jr., and Cummings David., Multiple failure surfaces over dip-slip faults, Journal of Geotechnical Engineering, ASCE, Proc. Paper 18789, Vol. 110, No. GT5, pp. 616-627, 1984.
5) Onizuka, N., Hakuno, M., Iwashita, K. and Suzuki, T., Deformation in grounds and bedrock stress induced by reverse dip-slip faults, Journal of Applied Mechanics, JSCE, Vol. 2, pp. 533-542, 1999.
6) Meguro, K. and Tagel-Din, H., Applied element method for structural analysis: Theory and application for linear materials, Structural Eng./Earthquake Eng., JSCE, Vol. 17, No. 1, 21s-35s, 2000.
7) Tagel-Din, H., A new efficient method for nonlinear, large deformation and collapse analysis of structures, Ph.D. thesis, Civil Eng. Dept., The University of Tokyo, 1998.
8) Meguro, K. and Tagel-Din H., A new efficient technique for fracture analysis of structures, Bulletin of Earthquake Resistant Structure Research Center, Institute of Industrial Science, The University of Tokyo, No. 30, 1997.
9) Wolf, J. P. and Song, Ch., *Finite element modeling of unbounded media*, John Wiley & Sons Ltd., Baffins Lane, Chichester, England, 1996.
10) Okada, Y., Surface deformation due to shear and tensile faults in half-space, *Bulletin of the Seismological Society of America*, Vol. 75, No. 4, pp. 1135-1154, August 1985.
11) Carlos Alberto Lazarte: *The response of earth structures to surface fault rupture*, Ph.D. thesis, University of California at Berkeley, 1996.
12) R. Ulusay, O. Aydan and m. Hamada: *The behaviour of structures built on active fault zones: Examples from the recent earthquakes of Turkey*, Seismic Fault Induced Failures, 1-26, 2001.
13) Naylor, M.A., Mandl. G., and Sijpesteijn, C.H.K.: *Fault geometries in basement-induced wrench faulting under different initial stress states*, Journal of Structural Geology, 8, No. 7, 737-752, 1986.